

Distinguishing nanobubbles from nanodroplets with AFM: the influence of vertical and lateral imaging forces

Hongjie An,^{*} Beng Hau Tan, and Claus-Dieter Ohl^{*}

*Cavitation Lab, Division of Physics and Applied Physics, School of Physical and Mathematical
Sciences, Nanyang Technological University, Singapore*

E-mail: hjan@ntu.edu.sg; cdohl@ntu.edu.sg

Abstract

The widespread application of surface-attached nanobubbles and nanodroplets in biomedical engineering and nanotechnology is limited by numerous experimental challenges, in particular, the possibility of contamination in nucleation experiments. These challenges are complicated by recent reports that it can be difficult to distinguish between nanoscale drops and bubbles. Here we identify clear differences in the mechanical responses of nanobubbles and nanodroplets under various modes of AFM imaging which subject the objects to predominantly vertical or lateral forces. This allows to distinguish between nanodroplets, nanobubbles, and oil covered nanobubbles in water.

Introduction

The nucleation of micro and nanoscale liquid drops and gaseous bubbles on surfaces has gathered significant interest in recent years for numerous applications.^{1–3} Nanodroplets are useful for

^{*}To whom correspondence should be addressed

biomolecular analysis and microfluidic reactors,⁴ while the decoration of surfaces with bubbles significantly reduces fluid drag in microchannels.⁵ Both nanobubbles and nanodroplets are produced by exchanging water with an organic solvent, such as ethanol, over a suitable surface.^{1-3,6} The nucleation mechanism of nanobubbles and nanodroplets appears to depend on the substantial difference in the solubility of gas (nanobubbles^{7,8}) or the desired liquid (nanodroplets⁶) in the water and solvent.

Given the similarity in their nucleation recipes, the contamination of exchange liquids may lead to the nucleation of both nanobubbles and nanodrops within a single experiment. It was recently reported that using disposable medical plastic syringes and cannulas to deliver liquids lead may lead to the contamination of nucleation experiments.⁹⁻¹² This contamination arises from the use of polydimethylsiloxane (PDMS) or other biologically-inert silicone oils to lubricate syringes and needles, in order to reduce discomfort during topical injections.^{13,14}

The issue of contamination contributes to reproducibility issues and conflicting results in the field of nanobubbles. It has been noted that the height and size distributions of nanobubbles characterised with atomic force microscopy (AFM) varies drastically between research groups,^{2,3} even though only widely-available liquids and atomically smooth substrates like highly oriented pyrolytic graphite (HOPG) are used in most such experiments.

Given the ease of contamination, experimental methods to distinguish polymeric liquid nanodroplets and gaseous nanobubbles are of urgent interest.^{2,3} Recently significant progress in this area has been made. Chan *et al.*¹⁵ used fluorescence microscopy to show that moving a contact line over a nanobubble deflated it upon exposure to the ambient atmosphere, while the contact line pinned strongly on a nanodroplet. Seo *et al.*¹⁶ distinguished between dye-covered bubbles and drops by identifying differences in fluorescence signals. However, the two tests either permanently alter the interfacial chemistry of the objects or destroy them upon identification. Moreover, the fact is that the vast majority of the literature characterise nanobubbles exclusively with AFM. It is therefore important to be able to make the distinction between nanobubbles, nanodroplets and contamination using AFM in particular, so as to allow researchers in this field an opportunity to

verify that their previously-published nucleation protocols are not contaminated.

In this article, we demonstrate that surface nanobubbles and nanodroplets on an atomically flat HOPG substrate can be differentiated through careful, non-destructive AFM characterization. We find distinct differences in the response of nanobubbles and nanodroplets in (a) PeakForce mode, in which the vertical imaging force can be carefully controlled; (b) contact mode, which delivers an invasive lateral force on the objects; and (c) force spectroscopy.

Results and discussion

Generation of nanobubbles and nanodroplets

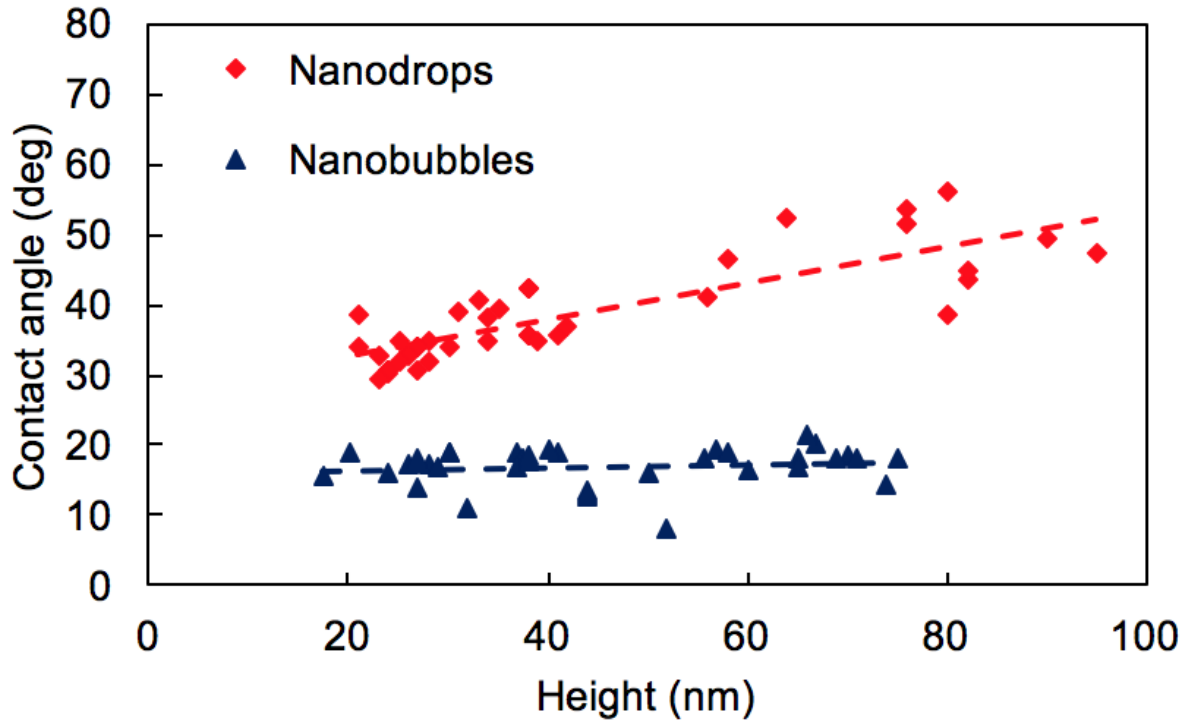


Figure 1: Nanoscopic contact angles of nanobubbles ($n = 36$) and nanodroplets ($n = 40$) as function of height. The angles are calculated by a least-square fit to a spherical cap. The nanoscopic contact angles of nanodroplets (red diamonds) increases with height, while nanobubbles (blue triangles) have a contact angle of $\approx 20^\circ$ which is independent of height.

To eliminate external contamination, we used unambiguous methods to nucleate nanobubbles

and nanodroplets, avoiding solvent exchange or plastic syringes. Hydrogen nanobubbles were electrolytically generated on HOPG, while nanodroplets were introduced by directly depositing a dilute solution of PDMS (see Materials and Methods).

A baseline distribution of sizes and contact angles was established by imaging nanobubbles and nanodroplets separately with tapping mode AFM. The nanoscopic contact angles of the objects were calculated by least-square fits of the cross-sectional profile to a spherical cap. As shown in Figure 1, the nanobubbles' fitted contact angles were virtually height-independent ($\theta \approx 20^\circ$), whereas the nanodroplets' contact angles increased ($30^\circ < \theta < 60^\circ$) with height. The contact angles are measured from the gas phase for nanobubbles and from the oil phase for the nanodroplets.

Morphology of nanobubbles and nanodroplets under varying peak force

The most direct way to compare nanobubbles and nanodroplets is to introduce them onto a common substrate. We first electrolysed water to generate bubbles, and later introduced oil drops by adding dilute oil solution, allowing both types of objects to appear on the same scan (Figure 2). We selected an area containing two nanodroplets and one nanobubble with similar lateral radii. To observe the effects of varying the imaging force on drops and bubbles, we used PeakForce tapping mode AFM. In this mode, the maximum vertical force on the cantilever is used as a feedback mechanism, allowing soft objects to be imaged with a *peak force* F_p that is typically of the order 0.1 to 1 nN, but can be controlled to an accuracy of ~ 10 pN.^{17–19}

We then performed successive AFM scans at $F_p = 0.5$ to 10 nN (Figures 2A-E). The morphology of nanodroplets and nanobubbles changed significantly with increasing F_p . At 0.5 nN, the height profiles of nanodroplets (Figures 2A and G) and nanobubbles (Figures 2A and H) were well-fitted to spherical caps. With increasing F_p , the nanobubble in Figure 2a became smaller in base radius and height, before disappearing completely at $F_p = 5.0$ nN. A nanodroplet also shrank in base radius and height with an increase in F_p , but at $F_p > 3$ nN appeared as a *sombrero*: a spherical cap sitting on a flat molecular layer. Remarkably, the molecular layer was highly resistant to vertical loading and remained in the height image at up to $F_p = 20$ nN, maintaining a thickness

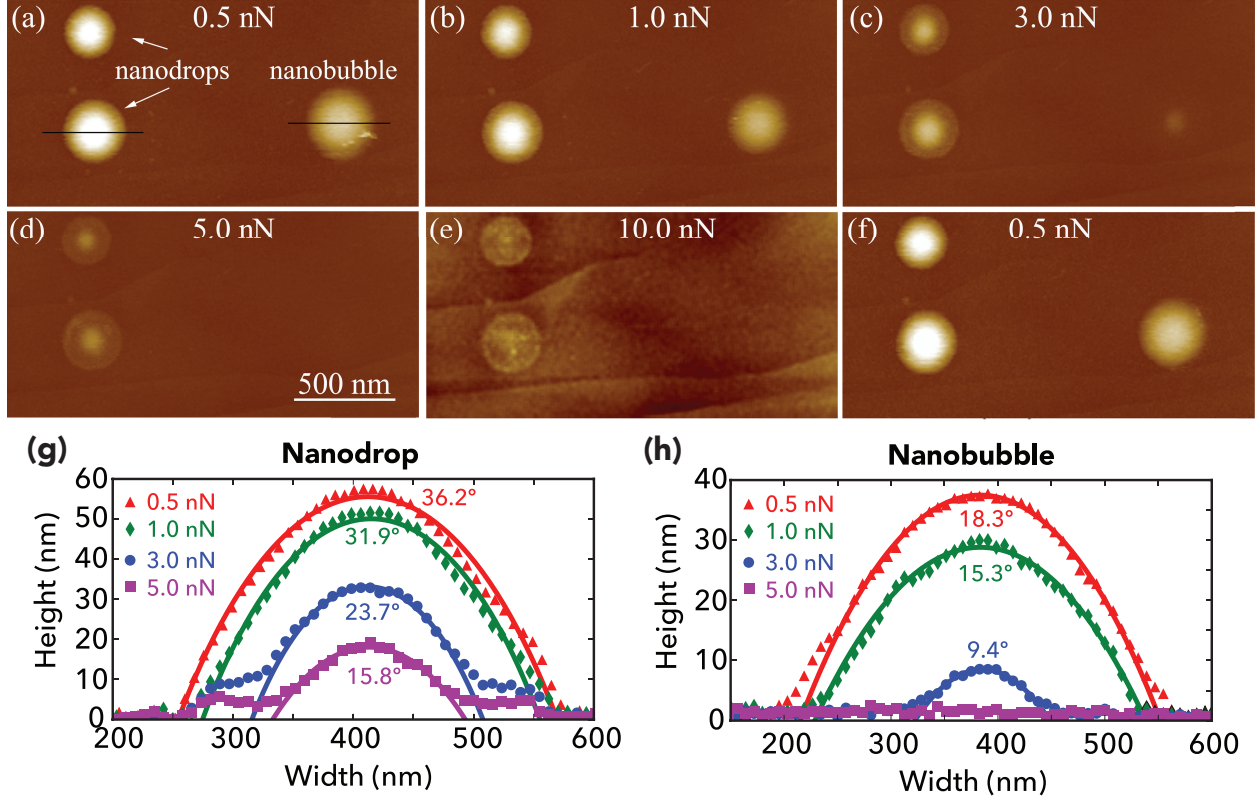


Figure 2: AFM height images of PDMS nanodroplets and a nanobubble in PeakForce mode. (A)-(E) Successive AFM images captured for peak forces $F_p = 0.5, 1.0, 3.0, 5.0$ and 10.0 nN. A final scan was taken at $F_p = 0.5$ nN, showing that the objects were not destroyed by the scanning. Scan size: $2 \mu\text{m} \times 1 \mu\text{m}$. Height scale: 50 nm for (A) - (D) and (F); 5 nm for (E). (G) Cross-sectional profiles of the bottom-left nanodroplet in (A)-(F). The nanodroplet adopts a sombrero shape at $F_p > 3$ nN, with a molecular layer of ~ 1 nm. (H) Cross-sectional profiles of the nanobubble. In (G) and (H) contact angles are indicated, and the lines are least-square fits to a spherical cap.

of 1-2 nm. Molecular layers of ~ 1 -2 nm thickness at the contact lines of spreading PDMS drops have previously been observed by ellipsometry,²⁰ though this layering is still not well understood. Finally, we note that neither bubbles nor drops were physically moved or destroyed by PeakForce imaging. When F_p was reduced from 10.0 to 0.5 nN, all the objects restored their original heights, base radii, and positions (Figure 2F).

The way we created the objects on the system – with bubbles created first, and drops introduced later – leaves open the possibility that the bubbles may have been coated with oils. To investigate this scenario, AFM scans were taken in PeakForce mode before and five hours after dilute oil solution was introduced into the system (Figure S1 in the Supporting Information). Some bubbles exhibited an increase of contact angle from 18-20° to 30-54° (Table S1, Figures S1-2). As surface nanobubbles are stable against diffusion for several weeks without significant changes to morphology, the difference in contact angle must arise only from the change in interfacial energy balance at the nanobubble’s three-phase line due to oil depositing on top of the nanobubbles. When F_p was increased incrementally, nanobubbles no longer disappeared from the scan image at $F_p = 5.0$ nN but maintained a nanometric layer (see Figures S1-2), similar to the oil nanodroplets.

The presence of a nanometric layer under strong AFM scanning is a tell-tale sign of contamination, resolving a contradiction raised by three recent papers imaging nanobubbles in PeakForce mode. Zhao *et al.*¹⁹ and Yang *et al.*¹⁷ found that nanobubbles disappeared from the scan image at $F_p = 1.25$ -2 nN, restoring their original heights when F_p was reduced to 0.2 nN. This agrees with our results. On the other hand, Walczyk *et al.*¹⁸ suggested that nanobubbles (~ 20 nm height, ~ 100 nm width) remained visible when F_p reached 27 nN. While the vast majority of work in the literature nucleated nanobubbles by solvent exchange or electrolysis,¹⁻³ they were able to nucleate the objects simply by delivering water with a disposable syringe. Our results suggest that the robust layers visible at high peak forces in Walczyk *et al.*¹⁸ were not nanobubbles, but polymeric contamination originating from plastic syringes.

Invasive contact mode scanning

Soft objects are usually imaged in non-invasive tapping or PeakForce mode AFM, rather than the conventional contact mode. In these modes, the tip height is adjusted rapidly (once in $100\ \mu\text{s}$ in PeakForce mode²¹) by a feedback mechanism to ensure that the tip and sample only contact intermittently. The imaging force is hence predominantly vertical, while avoiding strong lateral forces. In contrast, feedback in contact mode controls the cantilever deflection rather than the tip height, and this imparts a strong lateral force on the objects imaged. A schematic of these modes is shown in Figure S3.

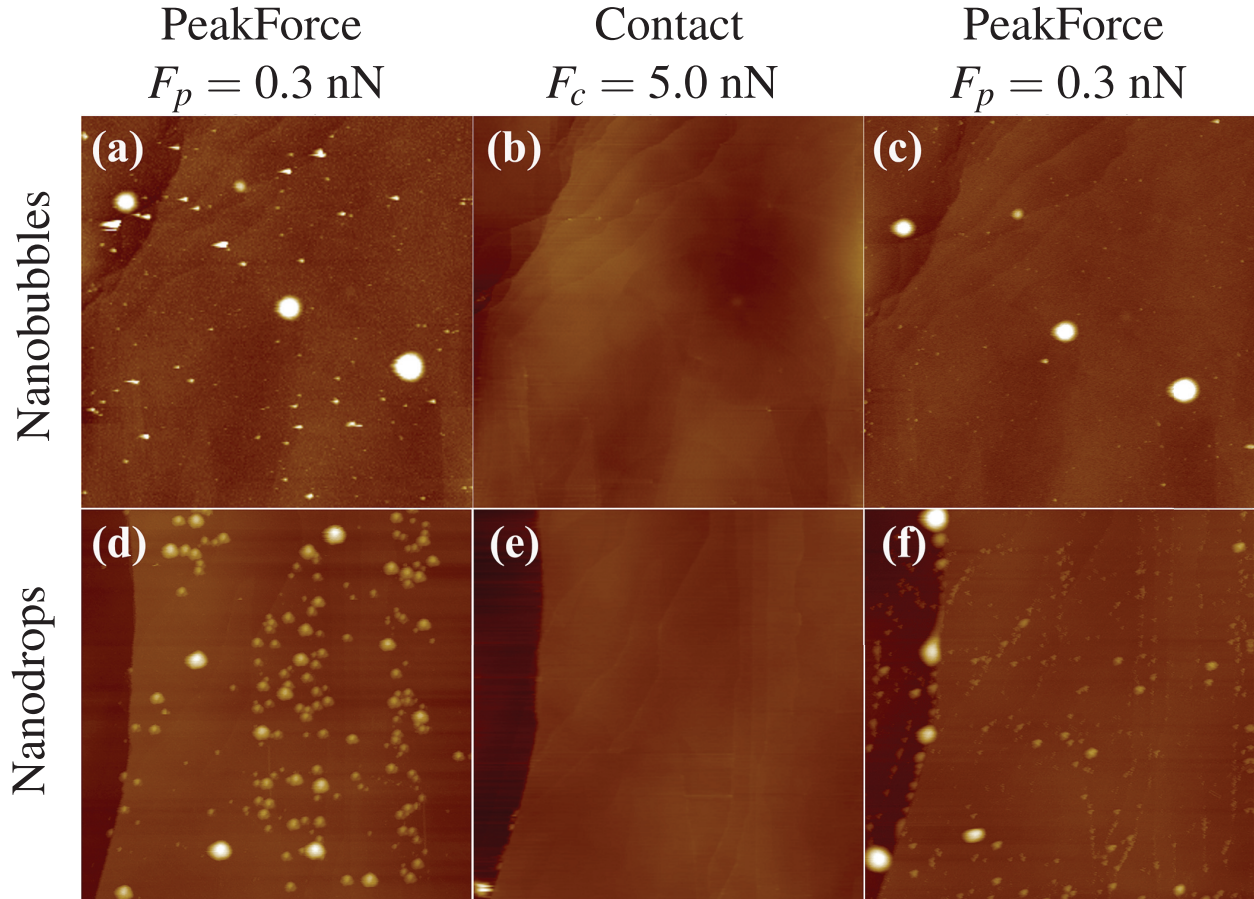


Figure 3: AFM height images of nanobubbles (A-C) and PDMS nanodroplets (D-F) before and after an invasive contact mode scan. The nanobubbles survive invasive scanning, while the nanodroplets' distribution is irreversibly altered, suggesting a drastic difference in substrate pinning. (A), (C), (D), and (F) are PeakForce mode height images captured at $F_p = 0.3\ \text{nN}$. (B) and (E) are captured by contact mode imaging (imaging force is $F_c = 5\ \text{nN}$). Scan size: $10\ \mu\text{m} \times 5\ \mu\text{m}$. Height scale: $50\ \text{nm}$ for (A-C); $100\ \text{nm}$ for (D-F).

To observe the influence of strong lateral deformation on nanobubbles and nanodroplets, we nucleated the objects separately on HOPG substrate and performed scans in PeakForce mode before (Figures 3A and D) and after (Figures 3C and F) a contact mode scan with an estimated imaging force of 5 nN (Figs. 3B and E). Before contact mode imaging, the deflection sensitivity (in units of m/volts) S_d was calibrated. The imaging force F_c was estimated as $F_c = kS_d(a_0 - a_v)$, where k is the spring constant of the cantilever, a_0 the set point and a_v the vertical deflection signal (both in volts) reading before the AFM was engaged. Figs. 3a-c show that nanobubbles on the substrate were neither moved nor destroyed by contact mode scanning. Some irregularly-shaped particles, likely dirt, were removed by the scanning. We were unable to unpin nanobubbles from the substrate, even when F_c was increased to ≈ 50 nN. On the contrary, the distribution of nanodroplets was completely altered at $F_c = 5.0$ nN, either by merging with other nanodroplets or being removed from the scan area (Figure 3F).

To understand why nanodroplets are unpinned and swept away in contact mode imaging, we make a few estimates. According to Young's equation, the contact angle of a surface-attached drop is defined only by the interfacial energies at its three phase line. The tip imparts a steady lateral force onto the drop, which deforms the drop from one side, changing its approaching and receding angles (Figure S3). The drop depins once the difference in angles – hysteresis – has reached a certain amount. Since this threshold is unknown, we instead exploit the fact that bubbles and drops possess an effective spring constant²² in the same order of magnitude as the surface tension of the object.²³ The force exerted on the drops can then be estimated from the distance of deformation x to be $F \sim \gamma_{pw}x$, where γ_{pw} is the PDMS-water interface tension. In the experiments, the PDMS-water interface has a surface tension of 40 mN/m,²⁴ and the nanodroplets have a typical base radius ~ 200 nm. Assuming that the maximum deformation of the drop is in the same order as the base radius, the threshold force to trigger the unpinning of the drop in contact mode AFM can be estimated to be 4 nN, in agreement with our experimental observation. On the other hand, in PeakForce mode, the intermittent contact between tip and object minimised contact angle hysteresis. Nanodroplets were thus able to withstand large vertical forces of ~ 10 nN without unpinning.

The force threshold required to unpin a nanobubble from its substrate remains unresolved. If nanobubbles and nanodroplets are pinned to their substrates by an identical force per unit length, and knowing that the interfacial energy of water-air is about double that of water-PDMS (72 versus 40 mJ/m²), the force threshold to unpin a bubble from the surface in contact mode should be approximately double that of a PDMS drop with same lateral size, i.e. $F_c \approx 10$ nN. However, we were unable to unpin nanobubbles at any imaging force in both imaging modes used here.

Force spectroscopy

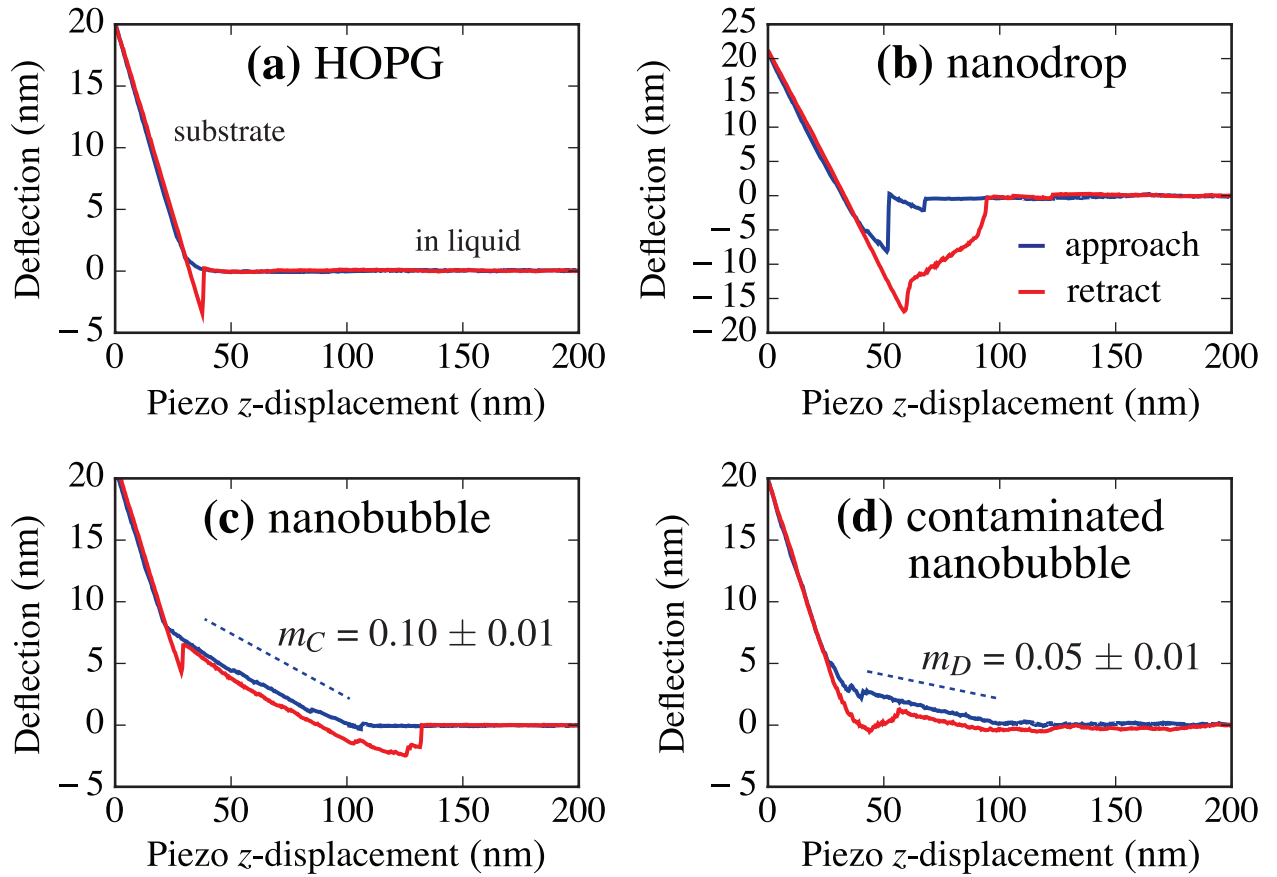


Figure 4: Cantilever deflection versus piezo z -displacement on the (A) HOPG substrate, (B) PDMS nanodroplet, (C) nanobubble and (D) nanobubble contaminated with PDMS. The approach curves are given in blue and the retraction curves are red. The tip-object slopes m on the approach curves in (C) and (D) were calculated with a least-square fit.

We also examined the tip-object interaction with AFM force spectroscopy. The tip-sample interaction is quantified by tracking the cantilever's vertical deflection as it moves down towards

(approach) and away (retract) from the sample. The force curves are read right-to-left. Figure 4A shows the deflection-displacement curve on the bare HOPG substrate. When the tip is far away from the substrate (‘in liquid’), the deflection is zero. The deflection then increases linearly as the tip comes into contact with the HOPG substrate (‘substrate’); the slope of the deflection-displacement curve gives a measure of the effective stiffness of the substrate.

We next show the force curves when the tip comes into contact first with a nanodroplet (Figure 4B) or a nanobubble (Figure 4C) before contacting the substrate. The tip-bubble interaction is characterised by a linear slope in the deflection-piezo displacement curve, which is consistent with theory²² and experiments.^{25,26} In our limited testing, this linear dependence occurs independent of the type of salt used in the electrolysis and probe wettability. Theory suggests that the tip-bubble interaction is linear²³ provided the magnitude of deformation by the tip is within a compliance regime.^{22,27} We assume that nanobubbles fall within this regime because the maximum deformation of a spherically-capped nanobubble is its height $h \sim 50$ nm, which is small compared to its radius of curvature $R_c \sim 1$ μ m. We note the caveat that in very pure systems, the initial contact between the AFM tip and the bubble is marked with a pronounced snap-in,²⁵ but this is suppressed in our case, perhaps due to disruption of electric double layer forces by electrolyte ions. However, the snap-in itself does not affect the linear dependence of the bubble-tip interaction. On the other hand, the tip-nanodroplet interaction is non-linear. Sharp kinks are observed in the approach curve in Figure 4b, representing a jump-to-contact with the substrate when the gradient of van der Waals forces between the oil and the tip overcomes the cantilever’s spring constant.²⁸

We were also able to distinguish between pure nanobubble and one that that was contaminated with a layer of oil. As with a pure nanobubble, the tip-contaminated bubble interaction is linear, but with a slope much smaller than for the pure nanobubble. Theory suggests that the slope of the deflection-displacement curve m is proportional to the surface tension of the interface γ .²³ This agrees well with our experimental observation that the ratio of the deflection curves on the contaminated bubble compared to the pure bubble (Figures 3C-D), $0.05/0.10$, is approximately the ratio of the surface tensions of water and PDMS, $m_C/m_D \approx \gamma_{\text{PDMS}}/\gamma_{\text{water}} = 5/9$.

Conclusions

In this Article, we identify a number of robust indicators to distinguish between nanobubbles and nanodroplets when they are imaged in AFM, such as differences in contact angles, force curves and response to different types of imaging forces. Our central result is that bubbles and drops exhibit very different responses under vertical and lateral forces. In PeakForce mode, we find that nanobubbles disappear cleanly from the AFM height images under large vertical imaging forces, but nanodroplets maintain a nanometric molecular layer under imaging forces in the order of tens of nN. In the standard contact mode AFM, we observe that nanobubbles are very strongly pinned onto their substrates and survive violent, lateral imaging forces of up to 50 nN without being moved or destroyed. Nanodroplets, on the other hand, are weakly pinned to their substrates and are easily depinned during contact mode imaging.

Our findings address a very urgent need in the field of nanobubbles to distinguish between gaseous objects and polymeric contamination which occurs easily during nucleation experiments. Although other methods of distinguishing between nanobubbles and contamination already exist, these tests are destructive and require specialised optical techniques inaccessible to the majority of research groups which image nanobubbles with AFM. We anticipate that our Article will equip researchers and engineers in the field of nanobubbles with a new perspective to judge previous work, as well as a diagnostic to verify the quality of their existing nucleation protocols.

Materials and methods

Nucleation of nanobubbles and nanodroplets

Hydrogen nanobubbles were generated by the electrolysis of aqueous solutions on highly ordered pyrolytic graphite (HOPG) substrate, the details of which are well-documented in previous work.^{29,30} Here, HOPG was used as the cathode and a copper wire as an anode within sodium phosphate solution (10 mM), and a DC voltage of 1.5 V was applied for 90 s.

To create oil nanodroplets, polydimethylsiloxane (PDMS) (Sylgard 184, Dow Corning, United States) was diluted with de-ionized water to 1:10,000 (vol/vol) (as described in⁹) and then directly deposited on HOPG.

AFM imaging

Atomic force microscopy scans were captured with a Bioscope Catalyst AFM (Bruker Corporation, United States). A V-shaped cantilever (SNL-10 A, Bruker) with a nominal spring constant of $k = 0.35 \text{ N m}^{-1}$ was used in an open liquid system. Before experiments, the AFM tip was treated with oxygen plasma for 15 s to render it hydrophilic, and the cantilever's spring constant was calibrated by a thermal method using built-in software.

To provide a baseline distribution of nanobubbles and nanodroplets that can be compared with previous work (Figure 1), nanobubbles and nanodroplets were independently imaged in the commonly-used tapping mode at a setpoint ratio of $A/A_0 = 0.8$, where $A_0 \approx 10 \text{ nm}$ is the free amplitude of the cantilever.

We studied the influence of primarily vertical imaging forces on the objects (Figure 2) by imaging in PeakForce tapping mode. In PeakForce mode, the cantilever is oscillated at a machine-selected frequency of about 1-2 kHz, far below its resonance in water ($\sim 30 - 40 \text{ kHz}$).²¹

Calculation of contact angle

All contact angles reported in the manuscript are calculated with a custom algorithm in Python with the scipy package. The left and right boundaries of the bubble were determined using a peak finding algorithm,³¹ before all the height points between the two detected boundaries were fitted using a standard least squares algorithm to a circle (spherical cap in axis symmetry). Finally, to determine the contact angle, a chord was constructed by interpolating points on the substrate outside the bubble. From the position of this chord relative to the circle, an elementary geometrical relation yields the contact angle.

Acknowledgement

We acknowledge funding from a competitive research programme under the auspices of the Singapore government's National Research Foundation (programme no. NRF-CRP9-2011-04). B.H.T. acknowledges financial support from the Agency of Science, Technology and Research in Singapore.

Supporting Information Available

The Supporting Information consists of a single file with four additional figures and one table.

This material is available free of charge via the Internet at <http://pubs.acs.org/>.

References

- (1) Craig, V. S. J. Very small bubbles at surfaces—the nanobubble puzzle. *Soft Matter* **2010**, *7*, 40–48.
- (2) Seddon, J. R. T.; Lohse, D. Nanobubbles and micropancakes: gaseous domains on immersed substrates. *J. Phys.: Condens. Matter* **2011**, *23*, 133001.
- (3) Lohse, D.; Zhang, X. Surface nanobubbles and nanodroplets. *Rev. Mod. Phys.* **2015**, *87*, 981–1035.
- (4) Zhang, X.; Lu, Z.; Tan, H.; Bao, L.; He, Y.; Sun, C.; Lohse, D. Formation of surface nanodroplets under controlled flow conditions. *Proc. Natl. Acad. Sci. U.S.A.* **2015**, *112*, 9253–9257.
- (5) Karatay, E.; Haase, A. S.; Visser, C. W.; Sun, C.; Lohse, D.; Tsai, P. A.; Lammertink, R. G. H. Control of slippage with tunable bubble mattresses. *Proc. Natl. Acad. Sci. U.S.A.* **2013**, *110*, 8422–8426.
- (6) Zhang, X. H.; Ducker, W. Formation of Interfacial Nanodroplets through Changes in Solvent Quality. *Langmuir* **2007**, *23*, 12478–12480.

- (7) German, S. R.; Wu, X.; An, H.; Craig, V. S. J.; Mega, T. L.; Zhang, X. Interfacial Nanobubbles Are Leaky: Permeability of the Gas/Water Interface. *ACS Nano* **2014**, *8*, 6193–6201.
- (8) Chan, C. U.; Ohl, C.-D. Total-Internal-Reflection-Fluorescence Microscopy for the Study of Nanobubble Dynamics. *Phys. Rev. Lett.* **2012**, *109*, 174501.
- (9) Berkelaar, R. P.; Dietrich, E.; Kip, G. A. M.; Kooij, E. S.; Zandvliet, H. J. W.; Lohse, D. Exposing nanobubble-like objects to a degassed environment. *Soft Matter* **2014**, *10*, 4947–4955.
- (10) An, H.; Liu, G.; Craig, V. S. J. Wetting of nanophases: Nanobubbles, nanodroplets and micropancakes on hydrophobic surfaces. *Adv. Colloid Interfac.* **2014**, *222*, 9–12.
- (11) Carr, J. A.; Nalwa, K. S.; Mahadevapuram, R.; Chen, Y.; Anderegg, J.; Chaudhary, S. Plastic-Syringe Induced Silicone Contamination in Organic Photovoltaic Fabrication: Implications for Small-Volume Additives. *ACS Appl. Mater. Interfaces* **2012**, *4*, 2831–2835.
- (12) Buettner, G. R.; Scott, B. D.; Kerber, R. E.; Mügge, A. Free radicals from plastic syringes. *Free Rad. Bio. Med.* **1991**, *11*, 69–70.
- (13) Siniawski, M. T.; Felts, J.; Kurilich, D.; Lopez, A.; Malik, A. Method for testing sliding frictional response of lubricious thin films used in plastic medical syringes. *Tribology S* **2015**,
- (14) Curtis, J.; Colas, A. In *Biomaterials Science (Third Edition)*; Ratner, B. D., Ed.; Academic Press, 2013; pp 1106–1116.
- (15) Chan, C. U.; Chen, L.; Arora, M.; Ohl, C.-D. Collapse of Surface Nanobubbles. *Phys. Rev. Lett.* **2015**, *114*, 114505.
- (16) Seo, D.; German, S. R.; Mega, T. L.; Ducker, W. A. The Phase State of Interfacial Nanobubbles. *J. Phys. Chem. C* **2015**, *119*, 14262–14266.

- (17) Yang, C.-W.; Lu, Y.-H.; Hwang, I.-S. Imaging surface nanobubbles at graphite-water interfaces with different atomic force microscopy modes. *J. Phys.: Condens. Matter* **2013**, *25*, 184010.
- (18) Walczyk, W.; Schön, P. M.; Schönherr, H. The effect of PeakForce tapping mode AFM imaging on the apparent shape of surface nanobubbles. *J. Phys. Cond. Mat.* **2013**, *25*, 184005.
- (19) Zhao, B.; Song, Y.; Wang, S.; Dai, B.; Zhang, L.; Dong, Y.; Lü, J.; Hu, J. Mechanical mapping of nanobubbles by PeakForce atomic force microscopy. *Soft Matter* **2013**, *9*, 8837–8843.
- (20) Heslot, F.; Fraysse, N.; Cazabat, A. M. Molecular layering in the spreading of wetting liquid drops. *Nature* **1989**, *338*, 640–642.
- (21) Kaemmer, S. B. Application note 133: introduction to Bruker’s ScanAsyst and PeakForce Tapping AFM Technology. Bruker Corporation, 2011.
- (22) Attard, P.; Miklavcic, S. J. Effective Spring Constant of Bubbles and Droplets. *Langmuir* **2001**, *17*, 8217–8223.
- (23) Attard, P. Direct Measurement of the Surface Tension of Nanobubbles. *arXiv:1505.02217 [cond-mat, physics]* **2015**,
- (24) Ismail, A. E.; Grest, G. S.; Heine, D. R.; Stevens, M. J.; Tsige, M. Interfacial Structure and Dynamics of Siloxane Systems: PDMS-Vapor and PDMS-Water. *Macromolecules* **2009**, *42*, 3186–3194.
- (25) Zhang, X. H.; Maeda, N.; Craig, V. S. J. Physical Properties of Nanobubbles on Hydrophobic Surfaces in Water and Aqueous Solutions. *Langmuir* **2006**, *22*, 5025–5035.
- (26) An, H.; Liu, G.; Atkin, R.; Craig, V. S. J. Surface Nanobubbles in Nonaqueous Media: Looking for Nanobubbles in DMSO, Formamide, Propylene Carbonate, Ethylammonium Nitrate, and Propylammonium Nitrate. *ACS Nano* **2015**, *9*, 7596–7607.

- (27) Chan, D.; Dagastine, R.; White, L. Forces between a rigid probe particle and a liquid interface: I. The repulsive case. *J. Colloid Interfac. Sci.* **2001**, *236*, 141–154.
- (28) Connell, S. D. A.; Allen, S.; Roberts, C. J.; Davies, J.; Davies, M. C.; Tendler, S. J. B.; Williams, P. M. Investigating the Interfacial Properties of Single-Liquid Nanodroplets by Atomic Force Microscopy. *Langmuir* **2002**, *18*, 1719–1728.
- (29) Wu, Z.; Chen, H.; Dong, Y.; Mao, H.; Sun, J.; Chen, S.; Craig, V. S.; Hu, J. Cleaning using nanobubbles: defouling by electrochemical generation of bubbles. *J. Colloid Interfac. Sci.* **2008**, *328*, 10–14.
- (30) Yang, S.; Tsai, P.; Kooij, E. S.; Prosperetti, A.; Zandvliet, H. J.; Lohse, D. Electrolytically generated nanobubbles on highly orientated pyrolytic graphite surfaces. *Langmuir* **2009**, *25*, 1466–1474.
- (31) Duarte, M. Notes on Scientific Computing for Biomechanics and Motor Control. <https://github.com/demotu/BMC>, 2015.

Graphical TOC Entry

